Strong magnetic anisotropy and unusual magnetic field reinforced phase in URhSn with a quasi-kagome structure

Yusei Shimizu,[1,*] Atsushi Miyake,[2] Arvind Maurya,[1] Fuminori Honda,[1] Ai Nakamura,[1] Yoshiki J. Sato,[1] Dexin Li,[1] Yoshiya Homma,[1] Makoto Yokoyama,[3] Yo Tokunaga,[4] Masashi Tokunaga,[2] and Dai Aoki[1]

[1]*Institute for Materials Research, Tohoku University, Oarai, Ibaraki 311-1313, Japan*

[2]*Institute for Solid State Physics, The University of Tokyo, Kashiwa, Chiba 277-8581, Japan*

[3]*Faculty of Science, Ibaraki University, Mito, Ibaraki 310-8512, Japan*

[4]*Advanced Science Research Center, Japan Atomic Energy Agency, Tokai, Ibaraki 319-1195, Japan*

(Received 5 June 2020; revised 31 August 2020; accepted 31 August 2020; published 9 October 2020)

The physical properties of URhSn with quasi-kagome structure are studied using single-crystalline samples via electrical resistivity, magnetic susceptibility, heat capacity, thermal expansion, and high-field magnetization measurements. Remarkable magnetic anisotropy is found in the ferromagnetic (FM) state below $T_C = 16$ K as well as in the ordered state between T_C and $T_O = 54$ K, where the easy and hard magnetization directions are the hexagonal [0001] and [10$\bar{1}$0] axes. In the paramagnetic state, the magnetic susceptibility shows a Curie-Weiss behavior; the Weiss temperatures are positive and negative for [0001] and [10$\bar{1}$0], respectively, indicating the presence of both FM and antiferromagnetic (AFM) correlations. The entropy release for $5f$ electrons is approximately $R\ln 3$ at T_O. The thermal expansion coefficient is strongly anisotropic around T_O between the hexagonal basal plane and the [0001] axis, indicating its remarkable anisotropic magnetoelastic response and uniaxial stress dependences. Interestingly, the magnetic field response of the higher-temperature ordered state is unusual: $T_O(H)$ increases and the heat-capacity jump is enhanced with the magnetic field for H || [0001]. Based on the established thermodynamic evidence for the second-order transition at $T_O(H)$, a plausible scenario is the occurrence of a canted AFM ordering or a conical state under magnetic fields, which is stabilized when coupled with field-induced magnetic moments along the [0001] axis. Another possibility is the occurrence of quadrupole ordering at $T_O(H)$.

DOI: 10.1103/PhysRevB.102.134411

I. INTRODUCTION

In solid-state physics, uranium compounds have attracted considerable interest because of their unusual properties, such as unconventional superconductivity [1–3], non-Fermi-liquid behavior due to quantum phase transitions [4], exotic Kondo effects [5], and metamagnetic instabilities [6–12]. Furthermore, uranium systems show exotic orders, e.g., multipole orders in UCu_2Sn [13–15], UNiSn [16], and UPd_3 [17,18], and the hidden order in URu_2Si_2 [3], whose order parameter has not been understood for more than three decades [19]. Meanwhile, geometrically frustrated magnetic materials are fascinating for the investigation of novel quantum states, such as spin liquids [20,21], the spin nematic state [22], and chiral magnetism [23]. Hence, a study of frustrated magnetic systems in uranium compounds with strong spin-orbit coupling would lead to a nontrivial research field.

The uranium-based UTX (T = transition metals, X = Al and Sn) system, which crystallizes in the hexagonal ZrNiAl-type structure (space group: $P\bar{6}2m$) without inversion symmetry in the crystal structure, is a good candidate for frustrated $5f$-electron systems. In particular, the ZrNiAl-type structure has a distorted kagome structure, which is comprised of a network of uranium triangular lattices [Figs. 1(a) and 1(b)]. Rare-earth-based ZrNiAl-type systems, such as CePdAl [24–29] and YbAgGe [30–32], show novel magnetic phase diagrams due to geometrical and magnetic frustration effects. Meanwhile, UTX compounds have provided various interesting properties due to the hybridization effects between $5f$ and conduction electrons [33]; furthermore, they have been investigated with a focus on their magnetic instability and quantum criticality [4]. For instance, UCoAl is a paramagnetic (PM) system at ambient pressure that exhibits an itinerant metamagnetic (first-order) transition at 8 kOe with an Ising-type moment (0.3 μ_B/U) [33,34]. It is considered that UCoAl is located in the vicinity of a tricritical point (TCP), as estimated at a negative pressure of -0.2 GPa [35]. Furthermore, the metamagnetic transition has been studied in detail based on tuning temperature (T), pressure (P), and magnetic field (H), demonstrating the wing structure in the T-P-H phase diagram [36–38]. Moreover, an isostructural ferromagnet URhAl exhibits a weak first-order ferromagnetic (FM) quantum phase transition at a critical pressure $P_c \sim 5$ GPa and non-Fermi-liquid behavior above P_c [39].

In the present study, we focus on URhSn, which shows successive phase transitions at $T_C = 16$ K and $T_O = 54$ K [40–43]. Previous studies have reported only the results of polycrystalline samples [40–43], where the transition at T_C was due to FM transition, whereas the nature of the ordered phase below T_O, which we call the *higher-T ordered*

*yuseishimizu@imr.tohoku.ac.jp

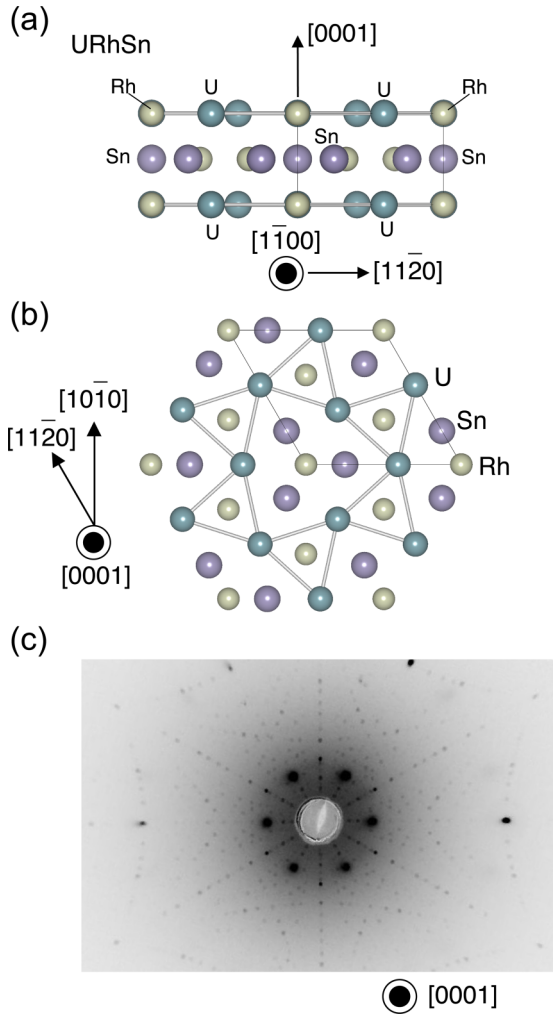

FIG. 1. The ZrNiAl-type hexagonal structure of URhSn, shown (a) for the (1$\bar{1}$00), which is equivalent to the (10$\bar{1}$0), and (b) for the (0001) planes. In the basal plane, the uranium atoms form a quasi-kagome structure. (c) Laue x-ray photograph for the (0001) plane of the annealed single-crystalline URhSn.

phase herein, has not yet been established. Interestingly, the higher-T ordered state may not have a simple magnetic origin, since no magnetic reflection has been observed below T_O from neutron scattering studies [42], and no internal field has been observed from ^{119}Sn Mössbauer spectroscopy [44]. Although isostructural UCoSn, URuSn, and UIrSn are all simple ferromagnets [40,41], URhSn shows an anomalous phase transition at T_O above T_C.

To understand the nature of the higher-T ordered phase in URhSn, more precise studies using single-crystalline samples are necessary. Recently, we have successfully grown single crystals of URhSn. Herein, we report the results of electrical resistivity, magnetic susceptibility, heat capacity, thermal expansion, and high-field magnetization experiments, and we discuss the origin of the unusual magnetic response of the higher-T ordered phase in URhSn.

II. EXPERIMENTAL PROCEDURES

Single-crystalline URhSn samples were grown using the Czochralski method in a tetra-arc furnace under an argon atmosphere. The obtained single crystals were annealed under high vacuum at 900 °C for ten days and 800 °C for seven days, and no remarkable difference was observed in overall magnetic properties, but the annealed URhSn showed sharper phase transitions at both T_C and T_O, as seen by the heat-capacity jump. In Fig. 1(c), a Laue photograph of the (0001) plane is shown. The clear Laue spots demonstrate the homogeneity of the single crystal obtained. In addition, a polycrystalline ThRhSn sample was synthesized by arc melting as a reference material for heat-capacity results.

Electrical resistivity and heat-capacity measurements were performed using a commercial physical property measurement system (PPMS, Quantum Design Inc.) at temperatures between 0.34 and 300 K. Here, the electrical resistivity measurements were performed for bar-shape samples using a standard four-probe ac method for the electric current along J || [0001] and [11$\bar{2}$0] at zero field, while the heat capacity measurements were performed using a thermal-relaxation method at zero and magnetic fields up to 90 kOe along the [0001]. Magnetization was measured at temperatures from 2 to 300 K in fields up to 70 kOe using a commercial magnetic property measurement system (MPMS, Quantum Design Inc.). Here, the temperature dependence of magnetization was measured under the field-cooled (FC) condition. High-field magnetization measurements of URhSn up to 560 kOe were performed using a nondestructive pulse magnet at temperatures from 1.4 to 100 K for the easy magnetization axis [0001]. The linear thermal expansion of URhSn was measured at zero field for $\Delta L/L$ || [10$\bar{1}$0], [11$\bar{2}$0], and [0001], using the active dummy gauge method, where strain gauges were glued on the rectangle-shaped sample, and a copper block was used as a reference. No superconductivity was observed in URhSn and ThRhSn down to 0.34 K via heat-capacity measurements.

III. RESULTS

A. Electrical resistivity

Figure 2(a) shows the temperature dependence of resistivity for annealed single-crystalline URhSn, at temperatures between 0.34 and 300 K, at zero field for the electric currents along the [0001] and [11$\bar{2}$0] axes. The remarkably anisotropic transport properties in URhSn may be related to the anisotropic Fermi surface in the PM and ordered states. The residual resistivity ratio (RRR) values for J || [0001] and J || [11$\bar{2}$0] are 22 and 11, respectively. Here, to minimize the effects of sample dependence, the bar-shaped samples were cut from a small sliced crystal of $\sim 1 \times 1 \times 0.2$ mm^3. The resistivity $\rho(T)$ shows clear kink anomalies at $T_O = 54$ K and $T_C = 16$ K, both of which are consistent with the results reported for polycrystalline samples [40]. Below T_C, the resistivity does not reflect $\rho(T) = \rho_0 + AT^2$ [Fig. 2(b)], which is expected for an itinerant ferromagnet at low temperatures [45]. By contrast, as shown in Fig. 2(c), the $\rho(T)$ in URhSn obeys the theory of anisotropic FM spin waves [43,46], i.e., $[\rho(T) = \rho_0 + A_{FM}T^2 e^{-\Delta/T} + B_{ph}T^5]$, where the Δ and the

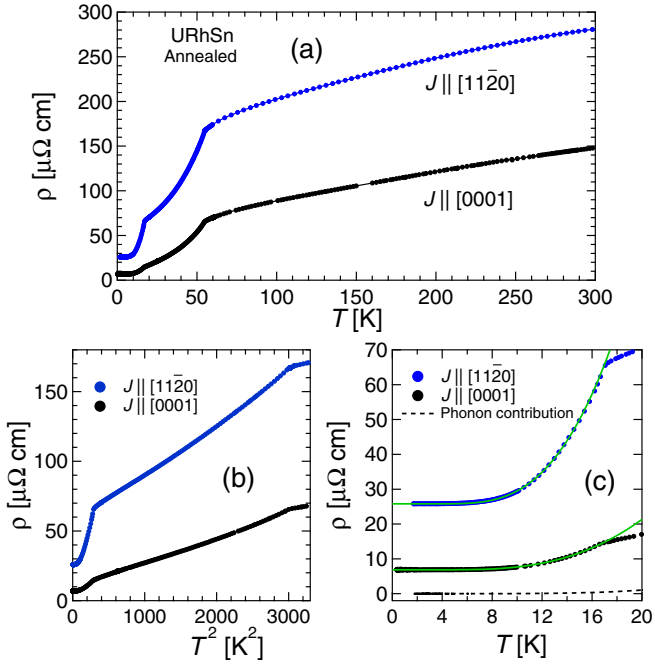

FIG. 2. (a) The temperature dependence of electrical resistivity $\rho(T)$ for the annealed single-crystalline URhSn at zero field for electric currents along J || [11$\bar{2}$0] and [0001]. (b) $\rho(T)$ vs T^2. (c) $\rho(T)$ below 20 K, where the solid line is the fitting result assuming the anisotropic FM spin wave, and the phonon contribution is derived from the resistivity data of a polycrystalline ThRhSn.

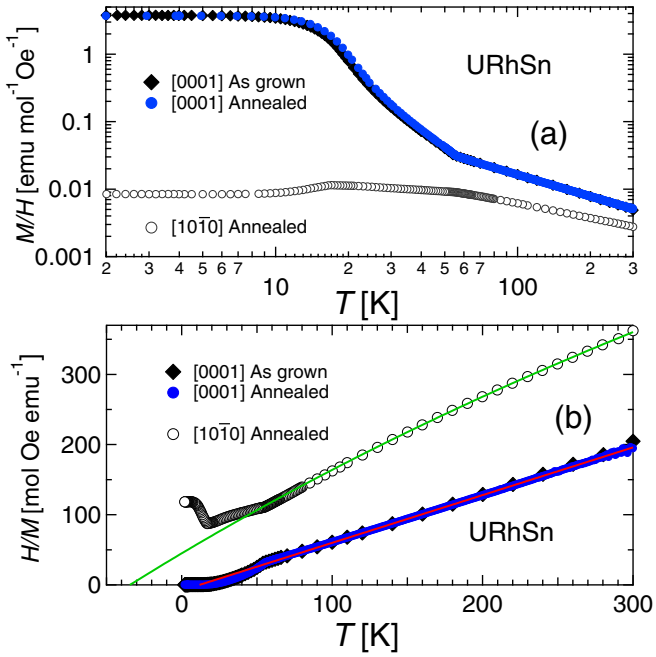

FIG. 3. (a) $M(T)/H$ of the annealed URhSn at 2 kOe under the FC condition for the [0001] and [10$\bar{1}$0] axes in logarithmic scales. (b) The inverse susceptibility $H/M(T)$ of URhSn for [0001] and [10$\bar{1}$0], where the solid lines are the results of fitting (see text). Here, the data for the as-grown sample are also plotted for [0001].

$B_{\rm ph}T^5$ term are the energy gap of a spin wave and the phonon contribution, respectively. We assume that the phonon contribution in URhSn is the same as for nonmagnetic ThRhSn, and we use the coefficient of $B_{\rm ph}$ obtained from the resistivity data of polycrystalline ThRhSn [the dotted curve in Fig. 2(c)]. At low temperatures below 15 K, the residual resistivity ρ_0, coefficient $A_{\rm FM}$, and Δ values obtained are $\rho_0 = 6.87\ \mu\Omega\,{\rm cm}$, $A_{\rm FM} = 0.146\ \mu\Omega\,{\rm cm\,K^{-2}}$, and $\Delta = 29.4$ K for J || [0001], and $\rho_0 = 25.8\ \mu\Omega\,{\rm cm}$, $A_{\rm FM} = 0.893\ \mu\Omega\,{\rm cm\,K^{-2}}$, and $\Delta = 31.9$ K for J || [11$\bar{2}$0]. These results indicate that the gap of the FM spin wave, Δ, does not depend on the direction of electric current, while the $A_{\rm FM}$ and ρ_0 are anisotropic over the two examined directions of current.

In addition, $\rho(T)$ is nearly quadratic in the higher-T ordered phase in a wide T window ($20 < T < 40$ K) [Fig. 2(b)] [43], although the origin of this behavior is still unclear.

B. Magnetic susceptibility and inverse susceptibility

Figure 3(a) shows the temperature dependence of the magnetization divided by the magnetic field, M/H, of URhSn measured at 2 kOe, applied along the hexagonal [0001] and [10$\bar{1}$0] axes under the FC condition. At approximately 20 K, the M || H value becomes considerably large for H || [0001] upon cooling due to the FM transition, which is consistent with previously reported results for polycrystalline samples [40,41,43]. A significant anisotropy of $\chi_c/\chi_a \sim 3$ was observed in the PM state above $T_{\rm O}$, where χ_c and χ_a are the magnetic susceptibilities along the [0001] and [10$\bar{1}$0] axes. Here, the magnetic susceptibility can be defined as $\chi = M/H$ in the PM and higher-T ordered states, as the $M(H)$ curves are almost linear between 30 and 300 K, in low magnetic fields below ~50 kOe, for both easy and hard magnetization axes. In the FM state, the anisotropy becomes extremely large, compared with those in the higher-T ordered phase and the PM state. This remarkable anisotropic FM state is similar to that observed in URhAl, which also has the ZrNiAl structure [47–49].

Figure 3(b) shows the inverse susceptibility $1/\chi(T) = H/M(T)$ of URhSn along H || [0001] and H || [10$\bar{1}$0]. The $1/\chi(T)$ data for H || [0001] above ~140 K are well described by the Curie-Weiss law, i.e., $\chi(T) = \frac{C_{\rm CW}}{T-\Theta_{\rm W}}$, where $C_{\rm CW}$ and $\Theta_{\rm W}$ are the Curie constant and Weiss temperature, respectively. For H || [0001], the effective moment and Weiss temperature obtained were $\mu^c_{\rm eff} \sim 3.4\mu_{\rm B}$ and $\Theta^c_{\rm W} \sim 12$ K, respectively. Meanwhile, $1/\chi(T)$ data for H || [10$\bar{1}$0] cannot be described by the Curie-Weiss law due to the presence of a non-negligible T-independent value. Therefore, we analyzed using the modified Curie-Weiss law $\chi(T) = \chi_{\rm const.} + \frac{C_{\rm CW}}{T-\Theta_{\rm W}}$, where $\chi_{\rm const} = 0.000\,54$ emu/mol is a T-independent value that includes the Van Vleck term, the Pauli PM contribution, and the diamagnetism of core electrons. The effective moment and Weiss temperature obtained for H || [10$\bar{1}$0] were $\mu^a_{\rm eff} \sim 2.4\mu_{\rm B}$ and $\Theta^a_{\rm W} \sim -34$ K, respectively.

The results above suggest that an FM interaction exists for H || [0001], whereas an antiferromagnetic (AFM) interaction exists for H || [10$\bar{1}$0].

C. Magnetization for easy axis

In Fig. 4, we plot the temperature dependence of the magnetization $M(T)$ for URhSn, measured at 10, 30, 50, and

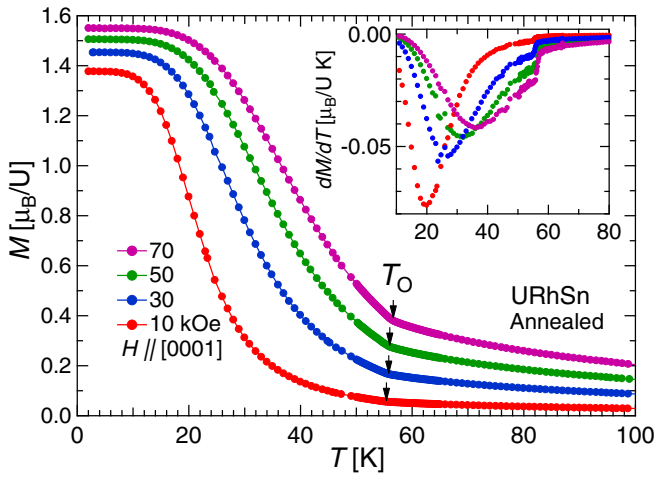

FIG. 4. The magnetization $M(T)$ of the annealed single-crystalline URhSn, measured at 10, 30, 50, and 70 kOe for the easy magnetization axis [0001] under the FC condition. The inset shows the temperature derivative of magnetization, dM/dT.

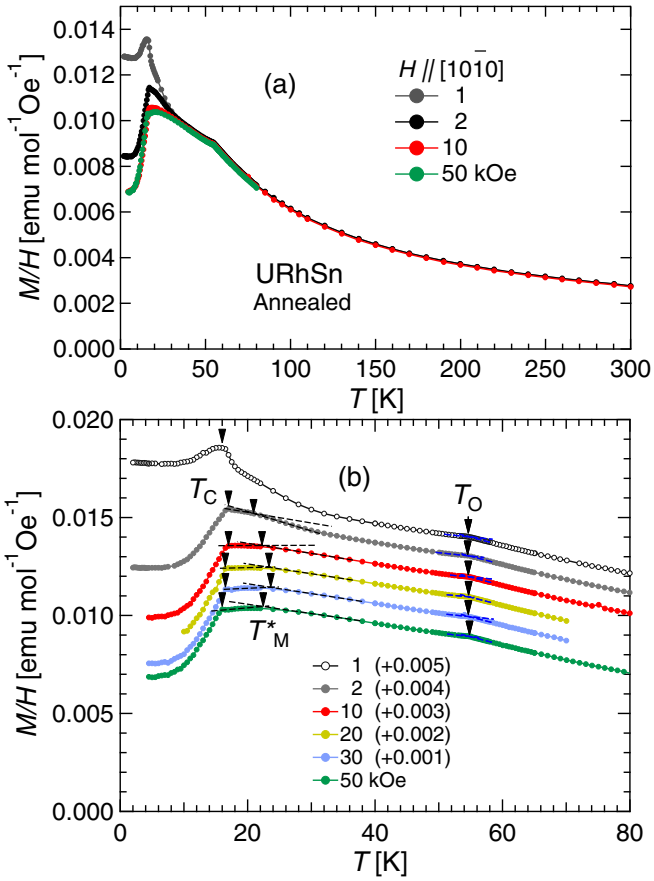

FIG. 5. (a) $M(T)/H$ for the annealed single-crystalline URhSn at 1, 2, 10, and 50 kOe applied along the hard magnetization axis [10$\bar{1}$0] under the FC condition. (b) The enlarged $M(T)/H$ measured at 1, 2, 10, 20, 30, and 50 kOe (with shifted traces), where arrows indicate the FM transition at T_C, the broad anomaly at T_M^*, and the higher-T order at T_O.

70 kOe along the easy magnetization axis of [0001] under the FC condition. At T_O, a kink anomaly was observed in $M(T)/H$. At low temperatures in the FM state, the induced moment at 70 kOe is 1.5 μ_B/U. Interestingly, the anomaly at T_O becomes sharper with increasing field as shown in the temperature derivative of magnetization [Fig. 4 (inset)], unlike that of the FM transition at T_C, which broadened with increasing field. Neither hysteresis nor steplike behaviors were observed for $M(T)$, suggesting that the phase transition at T_O is of second order.

D. Magnetization for the hard axis

Figure 5(a) shows the temperature dependence of the magnetic susceptibility in the form of M/H versus T for annealed URhSn for the hard magnetization axis of [10$\bar{1}$0], measured at 1, 2, 10, and 50 kOe. In Fig. 5(b), we present the enlarged data (shift values are indicated) to depict observed anomalies for clarity. Furthermore, we measured the temperature dependence of the magnetic susceptibility for H || [11$\bar{2}$0] (another hard magnetization axis, not shown). In the PM and the higher-T ordered states, the magnetic susceptibility is almost isotropic between [10$\bar{1}$0] and [11$\bar{2}$0]. At T_O, a clear kink anomaly was observed in $\chi(T)$, and interestingly, $\chi(T)$ continues to increase with decreasing T for $T_C < T < T_O$. Such a behavior differs from that of a collinear AFM state, in which $\chi(T)$ below the Néel temperature does not exceed the value in the PM state. The significant increase in $\chi(T)$ for $T < T_O$ is suppressed with increasing field. A broad anomaly is also seen in $M(T)/H$ at 22–23 K, defined as T_M^* [Fig. 5(b)], which may be related to the development of the FM fluctuations. A kink was observed at T_C as well, and $\chi(T)$ decreases upon cooling below T_C. This might imply that the FM ordering with the [0001] spin component is accompanied by a slightly canted FM state, where the magnetic moments might be tilted to the hexagonal basal plane, although such a signature has not yet been reported in neutron scattering experiments at zero field [42]. To verify this possibility, further studies using microscopic probes, such as neutron scattering and NMR experiments, are necessary.

E. $M(H)$ curves in low fields

Figure 6(a) shows the magnetization curve $M(H)$ measured in the FM state at 4.2 and 13 K, in the higher-T ordered phase at 25 K, and in the PM state at 60 K under fields along [0001]. Furthermore, in Fig. 6(b), the $M(H)$ curves for [10$\bar{1}$0] measured at 4.2, 25, and 60 K are shown. For all temperatures, the easy magnetization direction was [0001] in URhSn. A remarkable magnetic anisotropy was found between [0001] and [10$\bar{1}$0] below T_O ($M_{[0001]}/M_{[10\bar{1}0]} \sim 13$ at 25 K). In addition, at 4.2 K, the FM moment is $M \sim 1.5$ μ_B/U for [0001] at 55 kOe, with a particularly large anisotropy of $M_{[0001]}/M_{[10\bar{1}0]} \sim 25$. In the higher-$T$ ordered state ($T = 25$ K), $M(H)$ exhibits a convex curve for [0001], whereas the $M(H)$ curve above 40 K is almost linear in low fields, as shown later in the high-field magnetization results. In the PM state ($T = 60$ K), the $M(H)$ curves are also linear up to 55 kOe for both [0001] and [10$\bar{1}$0].

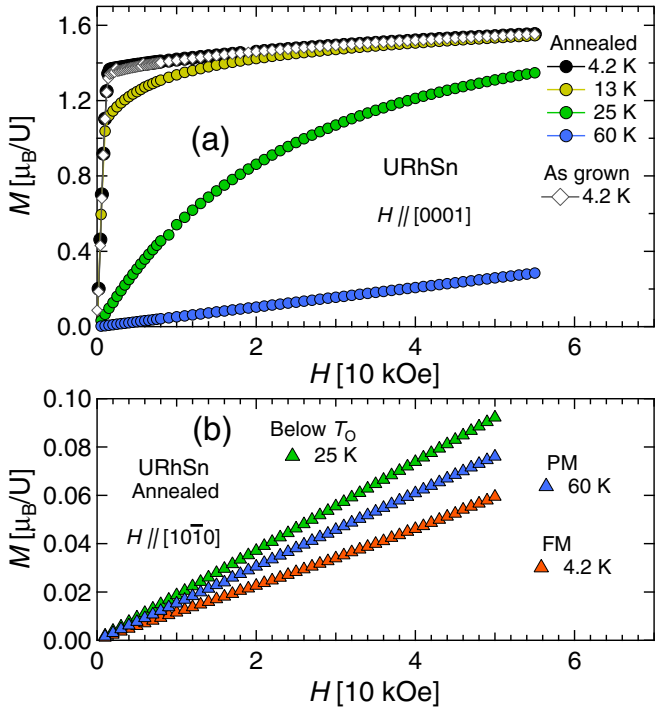

FIG. 6. (a) $M(H)$ curves of the annealed single-crystalline URhSn for [0001] at 4.2, 13 ($T < T_C$), 25 ($T < T_O$), and 60 K in the paramagnetic (PM) state, where diamond markers indicate the data for the as-grown sample. (b) $M(H)$ curves of the annealed single-crystalline URhSn for [10$\bar{1}$0] at 4.2, 25, and 60 K.

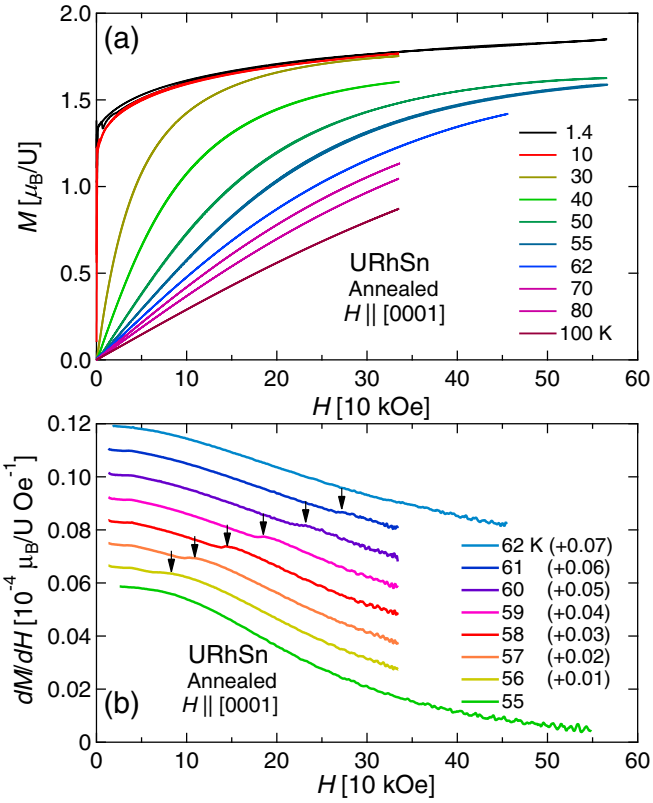

FIG. 7. (a) The magnetization curves for the annealed single-crystalline URhSn up to 560 kOe for [0001] at 1.4, 10, 30, 40, 50, 55, 62, 70, 80, and 100 K. (b) The differential magnetic susceptibility, dM/dH, at temperatures from 55 to 62 K (in 1 K steps) for [0001]. Here, the vertically shifted values are indicated for clarity.

F. High-field $M(H)$ curves

Additionally, we performed high-field magnetization measurements for URhSn using a pulse field magnet. Figure 7(a) shows $M(H)$ curves up to 560 kOe in URhSn for the easy magnetization axis [0001], measured at several temperatures from 1.4 to 100 K. As discussed above, the FM moment saturates gradually around 200 kOe along the easy magnetization direction. The magnetization curve up to at least 560 kOe does not show any anomaly except for the initial magnetization. Such a behavior may suggest a canted magnetic structure even in the FM state, which is supported by the fact that $M(T)/H$ decreases upon cooling below T_C for [10$\bar{1}$0] [Fig. 5(b)]. Figure 7(b) shows the differential magnetic susceptibility curves as a function of H at temperatures from 55 to 62 K. At 55 K, $dM(H)/dH$ decreases monotonically with increasing field, showing no anomaly. Furthermore, we confirmed the absence of an anomaly at 55 K up to 560 kOe [Figs. 7(a) and 7(b)]. By contrast, from 56 to 61 K, a hump anomaly appeared in $dM(H)/dH$, and it shifted toward the high-field region with increasing temperature. At 62 K, there is no anomaly up to 450 kOe. As will be discussed later based on the H-T phase diagram, the observed anomaly is related to the field-reinforced behavior of $T_O(H)$.

G. Heat capacity and 5f-electron contribution

Next, we analyzed the heat capacity $C(T)$ of URhSn. Figure 8 shows the temperature dependence of $C(T)/T$ for the annealed single crystal of URhSn on a semilogarithmic scale. The heat capacity of the polycrystalline ThRhSn is also plotted as a nonmagnetic reference material. The inset shows the low-T heat capacity for the as-grown single-crystalline URhSn and the polycrystalline ThRhSn below 2 K. The low-T C/T value is enhanced for URhSn (12 mJ K^{-2} mol^{-1}) due to the magnetic contribution, compared with the value

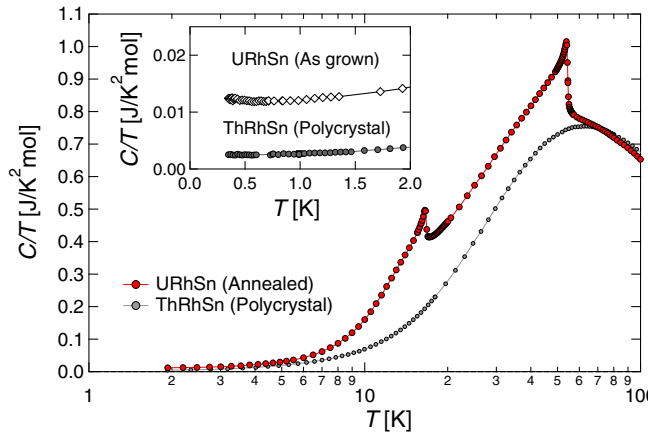

FIG. 8. The heat capacity $C(T)/T$ at zero field (in the semilogarithmic scale) for the annealed single-crystalline URhSn and polycrystalline ThRhSn. Inset: $C(T)/T$ below 2 K for the as-grown single-crystalline URhSn and polycrystalline ThRhSn.

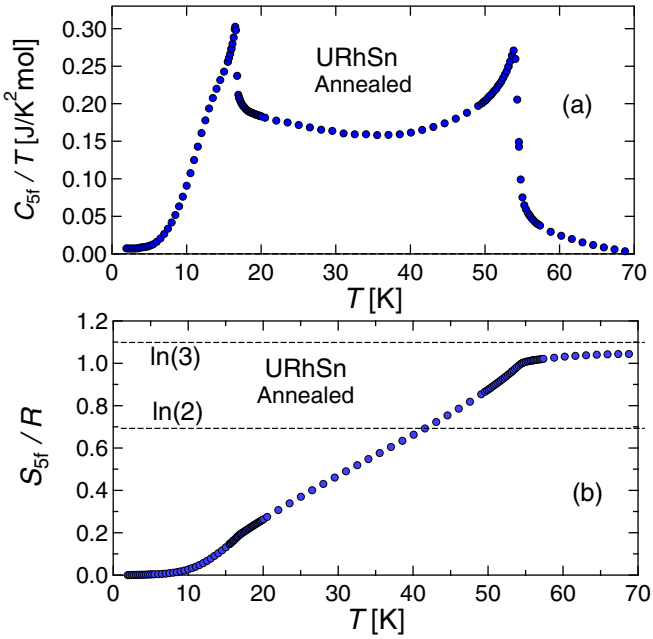

FIG. 9. (a) The magnetic contribution of heat capacity $C_{5f}(T)/T \equiv [C_{\mathrm{URhSn}}(T) - C_{\mathrm{ThRhSn}}(T)]/T$ in URhSn at zero field. (b) The obtained entropy of S_{5f} in URhSn, divided by the gas constant R.

of ThRhSn (2 mJ K^{-2} mol^{-1}). The magnetic contribution of $5f$ electrons in URhSn was obtained by subtracting the heat capacity of ThRhSn: $C_{5f}(T) \equiv C_{\mathrm{URhSn}}(T) - C_{\mathrm{ThRhSn}}(T)$ [Fig. 9(a)]. Using the $C_{5f}(T)/T$ data, we derived the magnetic entropy of $5f$ electrons in URhSn [Fig. 9(b)]. The entropy releases are approximately $0.2R$ ($\sim 0.3R \ln 2$) at T_{C} and R ($\sim R \ln 3$) at T_{O}.

H. Thermal expansion experiments

Figure 10(a) shows the temperature dependence of the linear thermal expansion in the annealed URhSn, $\Delta L/L$, measured at zero field for $\Delta L/L \parallel [10\bar{1}0]$, $[11\bar{2}0]$, and [0001]. In addition, in Fig. 10(b), the temperature dependence of the linear thermal expansion coefficient $\alpha_{\mathrm{L}}(T)$ in URhSn is plotted, which was obtained from $\Delta L/L$ data. The temperature dependence of the thermal expansion coefficient is fully isotropic in the hexagonal basal plane through T_{O} and T_{C}. Meanwhile, $\Delta L/L$ and $\alpha_{\mathrm{L}}(T)$ are highly anisotropic between the basal plane and the [0001] axis during the two phase transitions. In all directions, the $\alpha_{\mathrm{L}}(T)$ data showed a mean-field-like behavior and a λ-type peak at T_{O} and T_{C}, supporting the occurrence of successive second-order phase transitions. In addition, below T_{C}, the $\alpha_{\mathrm{L}}(T)$ data showed another broad anomaly at approximately 13 K [Fig. 10(b)], although the origin of this anomaly in the FM state is still unclear. We define the transition temperatures T_{O} and T_{C} as the peak positions of $\Delta\alpha_{\mathrm{L}}$, as indicated by upper arrows [Fig. 10(b)] and vertical dashed lines [Fig. 10(a)]. For the [0001] axis, the roughly estimated magnitude of jumps in the thermal expansion coefficient $\Delta\alpha_{\mathrm{L}}$ is indicated by dashed two-headed arrows. A similar estimation was applied to the $\Delta\alpha_{\mathrm{L}}$ data for the $[10\bar{1}0]$ axis.

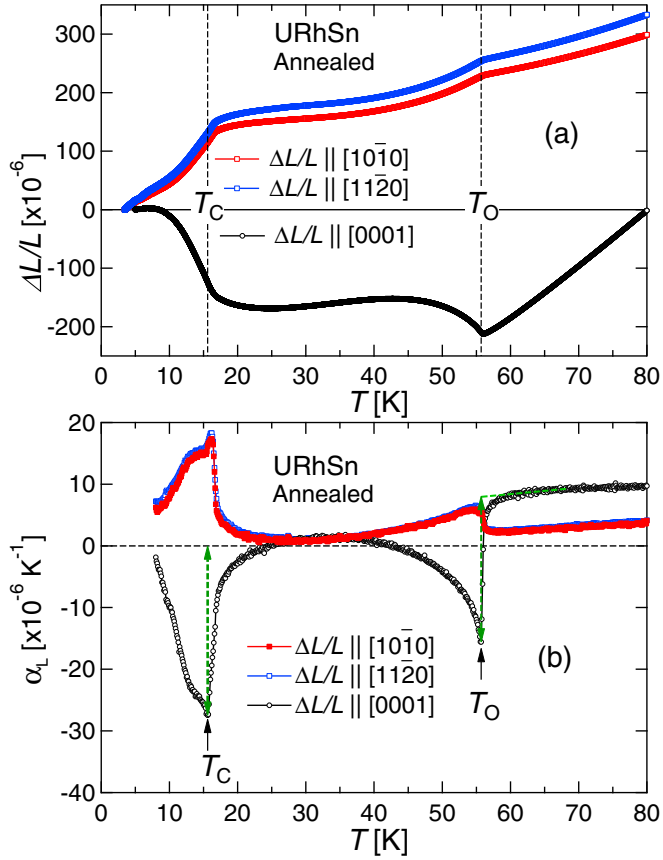

FIG. 10. (a) The temperature dependence of the linear thermal expansion $\Delta L/L$ for the $[10\bar{1}0]$, $[11\bar{2}0]$, and [0001] axes, for the annealed URhSn, measured at zero field. (b) The temperature dependence of the linear thermal expansion coefficient $\alpha_{\mathrm{L}}(T) \equiv d(\Delta L/L)/dT$. Here, the transition temperatures, T_{C} and T_{O}, defined as the peaks of $\Delta\alpha_{\mathrm{L}}(T)$, are indicated by upper arrows and dashed lines.

Using the thermal expansion coefficients, it is intriguing to estimate the uniaxial pressure dependence of the transition temperatures using the Ehrenfest relation. For the higher-T transition at T_{O}, we obtain $dT_{\mathrm{O}}/dP_i = V_{\mathrm{m}}\Delta\alpha_{\mathrm{L}}/(\Delta C/T_{\mathrm{O}}) = +0.7$ K/GPa and -3.9 K/GPa for the uniaxial stress (P_i) along $\Delta L/L \parallel [10\bar{1}0]$ and $\Delta L/L \parallel [0001]$, respectively [50]. Meanwhile, for the FM transition at T_{C}, we calculate $dT_{\mathrm{C}}/dP_i = V_{\mathrm{m}}\Delta\alpha_{\mathrm{L}}/(\Delta C/T_{\mathrm{C}}) = +6.5$ K/GPa and -10.3 K/GPa for the uniaxial stress along $\Delta L/L \parallel [10\bar{1}0]$ and $\Delta L/L \parallel [0001]$, respectively. It is noted that the anisotropy of the thermal expansion coefficient has greater significance for the higher-T transition (T_{O}) than for the FM transition (T_{C}), while the magnetization exhibits high anisotropy in the FM state below T_{C} [Fig. 3(a)]. In addition, the volume expansion coefficient ($\Delta\alpha_{\mathrm{V}}$) was estimated by applying the relation $\Delta\alpha_{\mathrm{V}} = 2\Delta\alpha_{\mathrm{L}}^{[10\bar{1}0]} + \Delta\alpha_{\mathrm{L}}^{[0001]}$. Using the Ehrenfest relation $dT_i/dP = V_{\mathrm{m}}\Delta\alpha_{\mathrm{V}}/(\Delta C/T_i)$, where $T_i = T_{\mathrm{O}}$ or T_{C}, we derive the pressure dependences (initial slopes) of T_{O} and T_{C} at ambient pressure. The obtained values of $dT_{\mathrm{O}}/dP = -2.5$ K/GPa and $dT_{\mathrm{C}}/dP = 2.7$ K/GPa are consistent with our pressure experiments [51].

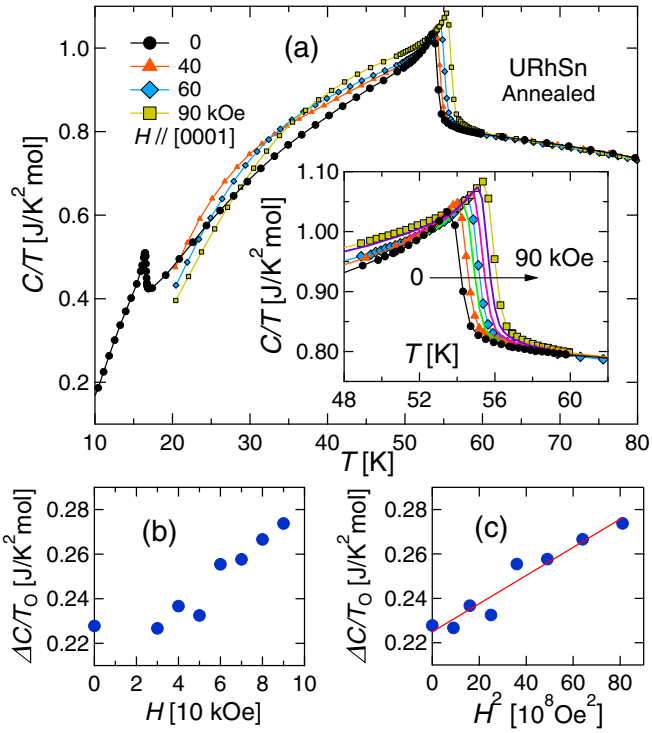

FIG. 11. (a) $C(T)/T$ of the annealed single-crystalline URhSn measured at 0, 40, 60, and 90 kOe for [0001], where the inset shows the enlarged figure around T_O (at 0, 40, 50, 60, 70, 80, and 90 kOe). The heat-capacity jump at T_O in URhSn, $\Delta C/T_O$, as a function of (b) magnetic field H and (c) H^2, where the solid line is the result of linear fitting.

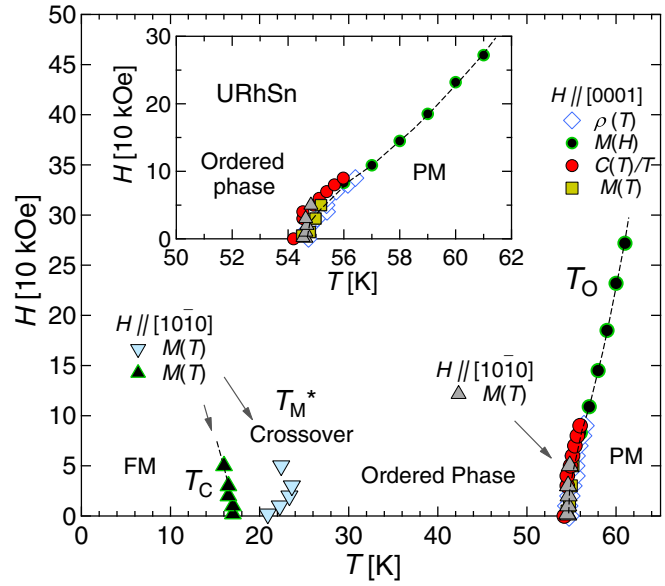

FIG. 12. H-T phase diagram of the annealed URhSn for [0001] and [10$\bar{1}$0], where the dashed lines are guides to the eyes. The inset shows the enlarged figure around $T_O(H)$.

I. Magnetic field dependences of $T_O(H)$ and heat-capacity jump

Next we focus on the magnetic field evolution of the transition at $T_O(H)$. Figure 11 shows the $C(T)/T$ measured in zero and several magnetic fields (40, 60, and 90 kOe) applied along the easy magnetization axis [0001]. The inset is an enlarged figure of $C(T)/T$ around the transition. Heat-capacity measurements in fields along the hard magnetization directions were not performed because of the difficulty due to strong magnetic torque effects. Interestingly, with increasing field, the heat-capacity jump in $C(T)/T$ at T_O becomes larger and sharper, and $T_O(H)$ shifts to a higher T with increasing field [Fig. 11(a) (inset)]. Figure 11(b) shows the field dependence of the heat-capacity jump $\Delta C/T_O$, considering the entropy conservation at T_O. The variation of heat-capacity jump at T_O is small below ~40 kOe, and $\Delta C/T_O$ is roughly proportional to H^2, as shown in Fig. 11(c). This proportionality is discussed phenomenologically in the following section.

J. H-T phase diagram

Figure 12 shows the obtained H-T phase diagram for URhSn. $T_O(H)$ increases with increasing field for [0001], and the evolution of the $T_O(H)$ line above 300 kOe is still unclear [52]. Meanwhile, $T_O(H)$ does not shift significantly for the hard magnetization axis [10$\bar{1}$0]. Furthermore, we plotted T_M^* [the broad anomaly in $M(T)/H$] and T_C for the hard magnetization axis of [10$\bar{1}$0]. In the case of a first-order transition (and TCP), a sharp peak anomaly is expected in $dM(H)/dH$; however, the dM/dH data did not show such behavior, suggesting that $T_O(H)$ maintains a second-order transition up to 300 kOe at the least. In general, when the symmetry of the ordered phase differs from that of the PM phase, the line of the ordered phase is distinguished from the PM state, and the line of the second-order phase transition should not terminate at a critical end point (CEP). Therefore, we consider that the line of phase transition may be located in magnetic fields higher than 560 kOe.

IV. DISCUSSION

In this section, we focus on the characteristics of the unusual phase transition at T_O in URhSn. Our experimental results indicate that the phase transition at T_O is a second-order phase transition, which is also strongly supported by thermodynamic considerations: $\frac{dT_O}{dH} > 0$ and $\Delta\left(\frac{\partial M}{\partial T}\right)\big|_{T=T_O} > 0$ satisfy the Ehrenfest relation, i.e., $\frac{dT_O}{dH} = -\Delta\left(\frac{\partial M}{\partial T}\right)/\Delta\left(\frac{C}{T}\right)$. Therefore, it is natural to consider that a symmetry breaking below T_O exists with an order parameter. The most prominent feature in URhSn is its unusual field response of T_O, which is not trivial. We explain the magnetic-field dependence of the transition temperature $T_O(H)$ phenomenologically in two general cases: the ordered states, in which (i) the time-reversal symmetry is broken with a magnetic order parameter of M_O; and (ii) the time-reversal symmetry is not broken with a quadrupole order parameter.

A. Magnetic order M_O below T_O

First, it is important to consider the magnetic susceptibility in the PM region. A negative Weiss temperature for H || [10$\bar{1}$0] indicates the presence of an AFM interaction, whereas a positive Weiss temperature for H || [0001] indicates the presence of an FM interaction. In addition, no remarkable anisotropy was observed in the hexagonal basal plane between

the $[10\bar{1}0]$ and $[11\bar{2}0]$ directions in the PM and higher-T ordered states. As shown in Fig. 1(a), the uranium atoms of URhSn form a triangular lattice with the distance of uranium atoms $d_{\text{U-U}} = 3.87$ Å, possessing three equivalent sites in the basal plane, whereas $d_{\text{U-U}} = 3.99$ Å for the [0001] axis [40].

The free energy for a simple system with AFM and FM interactions can be expressed using the Landau expansion with coefficients α, β, and γ, assuming $\alpha > 0$ and $\beta > 0$, as follows [53]:

$$F = \frac{\alpha}{2}[T - T_{\text{O}}(0)]M_{\text{O}}^2 + \beta M_{\text{O}}^4 + \gamma M_{\text{O}}^2 m^2 + \frac{\chi_0^{-1}}{2}m^2 - mH, \tag{1}$$

where M_{O} is the order parameter of the higher-T ordered phase, assuming an (undefined) AFM magnetic structure, and m is the uniform magnetization that couples to a magnetic field. In addition, χ_0 is the magnetic susceptibility when the magnetic order of M_{O} is absent.

By examining the stability condition of F for M_{O} and m, namely $\frac{\partial F}{\partial M_{\text{O}}} = \frac{\partial F}{\partial m} = 0$, one obtains the magnetic susceptibility as $\chi \equiv \frac{m}{H} = \chi_0(1 + 2\chi_0\gamma M_{\text{O}}^2)^{-1} \simeq \chi_0(1 - 2\chi_0\gamma M_{\text{O}}^2)$, near the transition temperature. In addition, M_{O}^2 is given as follows:

$$M_{\text{O}}^2 = -\frac{\alpha[T - T_{\text{O}}(0)] + 2\gamma\chi_0^2 H^2}{4\beta - 8\gamma^2\chi_0^3 H^2}. \tag{2}$$

The transition temperature $T_{\text{O}}(H)$ of the order parameter M_{O} can be obtained by setting the coefficient of M_{O}^2 in the free energy to zero:

$$T_{\text{O}}(H) = T_{\text{O}}(0) - \frac{2\gamma}{\alpha}(\chi_0 H)^2. \tag{3}$$

Importantly, if the coefficient γ for the $M_{\text{O}}^2 m^2$ term is *negative*, the transition temperature $T_{\text{O}}(H)$ increases with the magnetic field. In other words, applying fields (the presence of uniform magnetization) stabilizes the magnetic order of M_{O}. Simultaneously, the uniform magnetization $m \simeq \chi_0 H(1 - 2\chi_0\gamma M_{\text{O}}^2)$ increases below T_{O} upon cooling for $\gamma < 0$, as shown in Figs. 3(a) and 4. The heat capacity $C(T, H) = -T\frac{\partial^2 F}{\partial^2 T}$ near the transition temperature is derived for low fields H, using the expressions (1) and (2) for $F(T, H)$ and $M_{\text{O}}(T, H)^2$ [54]:

$$\frac{\Delta C}{T_{\text{O}}} \simeq \frac{\alpha^2}{8\beta}\left[1 + \frac{4\gamma^2\chi_0}{\beta}(\chi_0 H)^2\right]. \tag{4}$$

Thus, the above phenomenological arguments successfully explain $\Delta C/T_{\text{O}} \propto H^2$ behavior, as observed in Fig. 11(c).

Although the order parameter is not determined by our macroscopic measurements, we discuss the possible magnetic order in URhSn. Our heat-capacity data indicate that the second-order phase transition at T_{O} becomes pronounced by applying magnetic fields. To explain the anomalous field-reinforced order in URhSn, we phenomenologically proposed an AFM ordered state that stabilized in magnetic fields coupled with field-induced moments along the easy magnetization direction of [0001]. In addition, the high-field $M(H)$ curves did not exhibit any metamagnetic behavior up to 560 kOe in the higher-T ordered state at 50 K for the easy magnetization direction of [0001] [Fig. 7(a)]. In magnetic fields applied along [0001], a canted AFM ordering may occur in magnetic fields with no metamagnetic transition; the tilting of the canted AFM moments increases with the field until the magnetic moments are aligned parallel to the magnetic field direction. However, at zero field, the absence of an internal field below T_{O} should be considered to cancel out the internal field at the Sn site [Fig. 1(b)], which is halfway between two adjacent uranium quasi-kagome layers, as seen by previous zero-field Mössbauer spectroscopy [44]. Since there is no significant anisotropy in the basal plane in the higher-T ordered state, we speculate, for instance, that all-in and all-out 120° spin structures may stabilize an AFM triangular uranium lattice for two adjacent uranium layers.

We refer to an interesting system for comparison, $NpNiGa_5$, which exhibits successive magnetic transitions: AFM ($T^* = 26$ K) and FM ($T_{\text{C}} = 30$ K) transitions [55,56]. In $NpNiGa_5$, the canted AFM ordered state is embedded in the FM state, in contrast to the case of URhSn. Nevertheless, similar behaviors are observed in the easy magnetization axis of the tetragonal [001], i.e., an increase in magnetization $M(T)$ below T^* and the field-reinforced AFM transition temperature $T^*(H)$ [55].

Alternatively, the existence of both AFM (in the basal plane) and FM (along [0001]) correlations may result in a helimagnetic order (helicoidal state) in URhSn [57,58]. In this case, for magnetic fields applied perpendicular to the helicoidal plane, namely for the easy magnetization direction, a conical state would be stabilized, resulting in a magnetization curve with no metamagnetic transition. Therefore, a conical (FM helicoid) structure along the [0001] in magnetic fields may occur, which agrees with our high-field magnetization data. Meanwhile, the $M(H)$ curve is expected to indicate a metamagnetic transition when the helicoidal state becomes a fan structure for magnetic fields parallel to the helicoidal plane [59,60]. Further experiments using microscopic probes along with high-field experiments for hard magnetization axes are required to clarify the points above. In addition, our preliminary pressure experiments have revealed that $T_{\text{O}}(P)$ is suppressed with increasing P up to 5.9 GPa, while the Curie temperature $T_{\text{C}}(P)$ exhibits a broad maximum at $P \sim 4$ GPa, gradually approaching $T_{\text{O}}(P)$ [51]. The possible occurrence of the helimagnetic order in URhSn may result in a different type of quantum phase transition above ~ 6 GPa due to the competition between underlying FM and AFM interactions, in contrast to the wing structure observed in the isostructural ferromagnet URhAl [39] and other FM systems [4].

B. Quadrupole order below T_{O}

Another possible origin of the higher-T ordered state is multipole ordering, which is related to the $5f$-electron degrees of freedom. In particular, the field-reinforced behavior of the transition temperatures has been explained by the antiferroquadrupole ordering in CeB_6 and $PrPb_3$ [61,62]. In this case, the time-reversal symmetry is not broken, unlike the magnetic orders discussed above. In uranium systems, ferroquadrupole orderings have been observed in UCu_2Sn [13–15] and UNiSn [16], whereas antiferroquadrupole ordering has been observed in UPd_3 [17,18,63].

For URhSn, the entropy release at T_{O} is approximately $R\ln 3$ [Fig. 9(b)], although the crystal-electric-field (CEF)

level scheme in URhSn has not yet been clarified [64–66]. If a (pseudo)degenerate state exists in the CEF ground state with quadrupole degrees of freedom, a quadrupole ordering may occur to lift its degeneracy. To discuss this possibility, it is interesting to compare the behavior of thermal expansion in URhSn with the ferroquadrupole order in UCu_2Sn. Through the ferroquadrupole transition, UCu_2Sn exhibits significant anisotropic thermal expansion coefficients along the hexagonal $[10\bar{1}0]$ and [0001] axes [14]. It is also noted that the development of short-range ordering (fluctuations) is seen only along the [0001] axis for both UCu_2Sn and URhSn [Fig. 10(b)]. In UCu_2Sn, thermal expansions along the hexagonal $[10\bar{1}0]$ and $[11\bar{2}0]$ axes also show anisotropic behavior, $\Delta\alpha_L^{[10\bar{1}0]} < 0$ and $\Delta\alpha_L^{[11\bar{2}0]} > 0$, upon cooling through ferroquadrupole ordering, due to the cooperative Jahn-Teller effect [14]. As shown in Fig. 10(b), $\alpha_L(T)$ data along the $[10\bar{1}0]$ and $[11\bar{2}0]$ axes display isotropic behavior at around T_O in URhSn ($\Delta\alpha_L^{[10\bar{1}0]} \simeq \Delta\alpha_L^{[11\bar{2}0]} > 0$), in stark contrast to the behavior of UCu_2Sn [14].

At first glance, it may seem that these results for URhSn do not support the existence of ferroquadrupole ordering. However, thermal expansions along the hexagonal $[10\bar{1}0]$ and $[11\bar{2}0]$ axes may be isotropic because of the (twinned) elastic domain structure accompanied by the ferroquadrupole ordering. The observation of spontaneous distortion in UCu_2Sn likely implies that the domain size may not be small on a macroscopic scale in UCu_2Sn [14].

It is important to examine the thermal expansion of URhSn under uniaxial stress along the $[10\bar{1}0]$ and $[11\bar{2}0]$ axes to clarify the symmetry-breaking effect in the basal plane. However, it is unclear at this stage how much uniaxial stress would be necessary to *detwin* the domain of the higher-T order in URhSn. It is also important to examine the lattice constants and crystal structure through the higher-T phase transition using microscopic probes, such as low-T x-ray and neutron scattering experiments.

An antiferroquadrupole order is also possible. Crystal deformations in an antiferroquadrupole order would be expected to be smaller than deformations in a ferroquadrupole order, although any observation of crystal deformation on a macroscopic scale depends on the domain structure and the magnetoelastic coupling for each ordering. In the case of antiferroquadrupoles, applying a magnetic field is expected to induce a staggered magnetic multipole moment, including the dipole moment, because the field-induced mixing of the CEF states occurs between the quadrupole ground state and the CEF excited states at each U site. When these staggered magnetic multipole moments are stabilized due to AFM interactions, the transition temperature increases with the applied magnetic field, as shown in $T_O(H)$. However, the present magnetic susceptibility data indicate a positive Weiss temperature for H || [0001], indicative of the FM correlation between magnetic moments along this direction, in contrast to the aforementioned situation. Therefore, to clarify the possibility of antiferroquadrupole ordering, it is important to perform investigations using microscopic probes for URhSn. In particular, the azimuth-angle dependence of the resonant x-ray scattering intensity provides direct information regarding the presence of antiferroquadrupole ordering [67,68]. Furthermore, elastic neutron scattering experiments under magnetic fields along the [0001] axis can reveal whether the order parameter of the phase transition below T_O is the antiferroquadrupole order or not; the presence of the AFM ordered moment or the field-induced magnetic multipole moment may be directly detected as magnetic Bragg diffractions [69,70].

V. SUMMARY

In summary, we successfully grew single-crystalline URhSn, and we studied the nature of the successive phase transitions via transport, thermodynamic, and magnetic properties. Remarkable magnetic anisotropy was observed in the FM state ($T < T_C = 16$ K) and the higher-T ordered state ($T_C < T < T_O = 54$ K), where the easy and hard magnetization directions were along the [0001] and $[10\bar{1}0]$ axes, respectively. The resistivity is noticeably anisotropic for electric currents along the [0001] and $[11\bar{2}0]$ axes. In the PM state, the Curie-Weiss behavior was observed with FM and AFM correlations for [0001] and $[10\bar{1}0]$, respectively. The most remarkable feature is the observation of a field-reinforced second-order phase transition at T_O. Interestingly, the anomaly at T_O becomes pronounced with increasing field, which is evidenced thermodynamically, as shown in the heat-capacity jump ($\Delta C/T_O \propto H^2$). Thermal expansion data also support the occurrence of a second-order phase transition at T_O. The anisotropy of the thermal expansion coefficient is more prominent at the higher-T transition (T_O) than at the FM transition (T_C), while the magnetization exhibits greater anisotropy in the low-T FM state below T_C. Meanwhile, the large entropy release of $R\ln 3$ is observed at T_O, suggesting that the $5f$ electron degrees of freedom are related to this transition. A plausible scenario is the occurrence of a canted AFM order or a conical state under magnetic fields, which is stabilized through the coupling of field-induced magnetic moments along [0001]. Another possibility for the transition at T_O is quadrupole ordering in URhSn.

ACKNOWLEDGMENTS

We are grateful to T. Yanagisawa, Y. Ikeda, V. Taufour, and T. Sakakibara for valuable discussions. The present study was supported by Grants-in-Aid KAKENHI (Grants No. JP17K14328, No. JP18F18017, No. JP20K03851, and No. JP20K03854) from the Ministry of Education, Culture, Sports, Science and Technology (MEXT) of Japan. We acknowledge all the support from Institute for Materials Research, Tohoku University in growing uranium and thorium samples using the joint research facility at Oarai.

[1] H. R. Ott, H. Rudigier, Z. Fisk, and J. L. Smith, Phys. Rev. Lett. **50**, 1595 (1983).

[2] G. R. Stewart, Z. Fisk, J. O. Willis, and J. L. Smith, Phys. Rev. Lett. **52**, 679 (1984).

[3] T. T. M. Palstra, A. A. Menovsky, J. van den Berg, A. J. Dirkmaat, P. H. Kes, G. J. Nieuwenhuys, and J. A. Mydosh, Phys. Rev. Lett. **55**, 2727 (1985); W. Schlabitz, J. Baumann, B. Pollit, U. Rauchschwalbe, H. M. Mayer, U. Ahlheim, and C. D. Bredl, Z. Phys. B **62**, 171 (1986); M. B. Maple, J. W. Chen, Y. Dalichaouch, T. Kohara, C. Rossel, M. S. Torikachvili, M. W. McElfresh, and J. D. Thompson, Phys. Rev. Lett. **56**, 185 (1986).

[4] M. Brando, D. Belitz, F. M. Grosche, and T. R. Kirkpatrick, Rev. Mod. Phys. **88**, 025006 (2016).

[5] D. L. Cox and A. Zawadowski, Adv. Phys. **47**, 599 (1998).

[6] J. A. Mydosh, Adv. Phys. **66**, 263 (2017).

[7] J. J. M. Franse, H. P. van der Meulen, A. A. Menovsky, A. de Visser, J. A. A. J. Perenboom, and H. van Kempen, J. Magn. Magn. Mater. **90-91**, 29 (1990).

[8] A. de Visser, H. Nakotte, L. T. Tai, A. A. Menovsky, S. A. M. Menthink, G. J. Nieuwenhuys, and J. A. Mydosh, Physica B **179**, 84 (1992).

[9] M. Jaime, K. H. Kim, G. Jorge, S. McCall, and J. A. Mydosh, Phys. Rev. Lett. **89**, 287201 (2002).

[10] N. Harrison, M. Jaime, and J. A. Mydosh, Phys. Rev. Lett. **90**, 096402 (2003).

[11] W. Knafo, F. Duc, F. Bourdarot, K. Kuwahara, H. Nojiri, D. Aoki, J. Billette, P. Frings, X. Tonon, E. Lelièvre-Berna, J. Flouquet, and L.-P. Regnault, Nat. Commun. **7**, 13075 (2016).

[12] K. Mochidzuki, Y. Shimizu, A. Kondo, A. Matsuo, D. X. Li, D. Aoki, Y. Homma, F. Honda, J. Flouquet, D. Nakamura, S. Takeyama, and K. Kindo, Phys. Rev. B **100**, 165137 (2019).

[13] T. Suzuki, I. Ishii, N. Okuda, K. Katoh, T. Takabatake, T. Fujita, and A. Tamaki, Phys. Rev. B **62**, 49 (2000).

[14] I. Ishii, H. Higaki, T. Takabatake, H. Goshima, T. Fujita, T. Suzuki, and K. Katoh, Phys. Rev. B **68**, 144413 (2003).

[15] I. Ishii, K. Katoh, T. Takabatake, S. Hashio, A. Tamaki, and T. Suzuki, J. Phys. Soc. Jpn. **81**, 024602 (2012).

[16] T. Akazawa, T. Suzuki, H. Goshima, T. Tahara, T. Fujita, T. Takabatake, and H. Fujii, J. Phys. Soc. Jpn. **67**, 3256 (1998).

[17] Y. Tokiwa, K. Sugiyama, T. Takeuchi, M. Nakashima, R. Settai, Y. Inada, Y. Haga, E. Yamamoto, K. Kindo, H. Harima, and Y. Onuki, J. Phys. Soc. Jpn. **70**, 1731 (2001).

[18] H. C. Walker, K. A. McEwen, D. F. McMorrow, S. B. Wilkins, F. Wastin, E. Colineau, and D. Fort, Phys. Rev. Lett. **97**, 137203 (2006).

[19] J. A. Mydosh, P. M. Oppeneer, and P. S. Riseborough, J. Phys.: Condens. Matter **32**, 143002 (2020).

[20] P. A. Lee, Science **321**, 1306 (2008).

[21] L. Balents, Nature (London) **464**, 199 (2010).

[22] C. Lacroix, P. Mendels, and F. Mila, *Introduction to Frustrated Magnetism: Materials, Experiments, Theory*, Springer Series in Solid-State Sciences Vol. 164 (Springer, New York, 2011).

[23] M. Janoschek, M. Garst, A. Bauer, P. Krautscheid, R. Georgii, P. Böni, and C. Pfleiderer, Phys. Rev. B **87**, 134407 (2013).

[24] A. Dönni, G. Ehlers, H. Malett, P. Fischer, H. Kitazawa, and M. Zolliker, J. Phys.: Condens. Matter **8**, 11213 (1996).

[25] L. Keller, A. Dönni, H. Kitazawa, and B. van den Brandt, Appl. Phys. A **74**, s686 (2002).

[26] A. Oyamada, S. Maegawa, M. Nishiyama, H. Kitazawa, and Y. Isikawa, Phys. Rev. B **77**, 064432 (2008).

[27] H. Zhao, J. Zhang, S. Hu, Y. Isikawa, J. Luo, F. Steglich, and P. Sun, Phys. Rev. B **94**, 235131 (2016).

[28] K. Mochidzuki, Y. Shimizu, A. Kondo, S. Nakamura, S. Kittaka, Y. Kono, T. Sakakibara, Y. Ikeda, Y. Isikawa, and K. Kindo, J. Phys. Soc. Jpn. **86**, 034709 (2017).

[29] S. Lucas, K. Grube, C.-L. Huang, A. Sakai, S. Wunderlich, E. L. Green, J. Wosnitza, V. Fritsch, P. Gegenwart, O. Stockert, and H. v. Löhneysen, Phys. Rev. Lett. **118**, 107204 (2017).

[30] G. M. Schmiedeshoff, E. D. Mun, A. W. Lounsbury, S. J. Tracy, E. C. Palm, S. T. Hannahs, J.-H. Park, T. P. Murphy, S. L. Bud'ko, and P. C. Canfield, Phys. Rev. B **83**, 180408(R) (2011).

[31] Y. Tokiwa, M. Garst, P. Gegenwart, S. L. Bud'ko, and P. C. Canfield, Phys. Rev. Lett. **111**, 116401 (2013).

[32] J. K. Dong, Y. Tokiwa, S. L. Bud'ko, P. C. Canfield, and P. Gegenwart, Phys. Rev. Lett. **110**, 176402 (2013).

[33] V. Sechovsky and L. Havela, *Handbook of Magnetic Materials, Magnetism of Ternary Intermetallic Compounds of Uranium* (Elsevier Science, Amsterdam, 1998), Vol. 11, Chap. 1.

[34] A. V. Andreev, I. K. Kozlovskaya, N. V. Mushnikov, T. Goto, V. Sechovský, Y. Homma, and Y. Shiokawa, J. Alloys Compd. **284**, 77 (1999).

[35] N. V. Mushnikov, T. Goto, K. Kamishima, H. Yamada, A. V. Andreev, Y. Shiokawa, A. Iwao, and V. Sechovsky, Phys. Rev. B **59**, 6877 (1999).

[36] D. Aoki, T. Combier, V. Taufour, T. D. Matsuda, G. Knebel, H. Kotegawa, and J. Flouquet, J. Phys. Soc. Jpn. **80**, 094711 (2011).

[37] N. Kimura, N. Kabeya, H. Aoki, K. Ohyama, M. Maeda, H. Fujii, M. Kogure, T. Asai, T. Komatsubara, T. Yamamura, and I. Satoh, Phys. Rev. B **92**, 035106 (2015).

[38] L. Havela, A. V. Kolomiets, A. V. Andreev, J-C. Griveau, F. Honda, and Z. Arnold, J. Phys.: Condens. Matter **30**, 385601 (2018).

[39] Y. Shimizu, D. Braithwaite, B. Salce, T. Combier, D. Aoki, E. N. Hering, S. M. Ramos, and J. Flouquet, Phys. Rev. B **91**, 125115 (2015).

[40] T. T. M. Paltra, G. J. Nieuwenhuys, R. F. M. Vlastuin, J. van den Berg, and J. A. Mydosh, J. Magn. Magn. Mater. **67**, 331 (1987).

[41] V. H. Tran and R. Troć, J. Magn. Magn. Mater. **102**, 74 (1991).

[42] F. Mirambet, B. Chevalier, L. Fournès, J. Ferreira da Silva, M. A. Frey Ramos, and T. Roisnel, J. Magn. Magn. Mater. **140-144**, 1387 (1995).

[43] V. H. Tran, R. Troć, and D. Badurski, J. Alloys Compd. **219**, 285 (1995).

[44] R. Kruk, R. Kmieć, K. Łatka, K. Tomala, R. Troć, and V. H. Tran, Phys. Rev. B **55**, 5851 (1997).

[45] K. Ueda and T. Moriya, J. Phys. Soc. Jpn. **39**, 605 (1975).

[46] A. R. Mackintosh, Phys. Lett. **4**, 140 (1963).

[47] P. A. Veenhuizen, F. R. de Boer, A. A. Menovsky, V. Sechovsky, and L. Havela, J. Phys. **49**, C8-485 (1988).

[48] P. Javorský, L. Havela, F. Wastin, P. Boulet, and J. Rebizant, Phys. Rev. B **69**, 054412 (2004).

[49] T. Combier, Ph.D. thesis, CEA-Grenoble, 2014, https://tel.archives-ouvertes.fr/tel-01367953/document.

[50] Here, the cell volume is $187.6 \times 10^{-24}\text{cm}^3$ and the number of uranium atom in the formula unit of URhSn is $z = 3$ [40]; the molar volume is then $V_\text{m} = 62.53 \times 10^{-24} \times N_\text{A}\,\text{cm}^3\,\text{mol}^{-1}$, where $N_\text{A} = 6.022 \times 10^{23}\,\text{mol}^{-1}$ is the Avogadro number. And the values of heat-capacity jumps at zero field are $\Delta C/T_\text{O} = 0.23$ and $\Delta C/T_\text{C} = 0.10\,\text{J}\,\text{K}^{-2}\,\text{mol}^{-1}$ assuming entropy conservation for each transition.

[51] A. Maurya, F. Honda, Y. Shimizu, A. Nakamura, Y. J. Sato, Y. Homma, D. X. Li, and D. Aoki, JPS Conf. Proc. **29**, 014003 (2020).

[52] One may consider the possibility of a first-order phase transition or a TCP, where the second-order phase transition changes to a first-order one; in this case, the first-order phase transition may disappear at a critical end point (CEP) and the phase transition may become a crossover above the CEP.

[53] See, for example, P. M. Chaikin and T. C. Lubensky, *Principles of Condensed Matter Physics* (Cambridge University Press, Cambridge, England, 1995); J. C. Torédano and P. Torédano, *Landau Theory of Phase Transitions, The Application to Structural, Incommensurate, Magnetic and Liquid Crystal Systems*, Lecture Notes in Physics (World Scientific, Singapore, 1987).

[54] The heat capacity is obtained as $C = \frac{\alpha^2 T}{8\beta}(1 - \frac{2\gamma^2}{\beta}\chi_0^3 H^2)^{-2} \simeq \frac{\alpha^2 T}{8\beta}[1 + \frac{4\gamma^2\chi_0}{\beta}(\chi_0 H)^2]$. The heat-capacity jump at the transition is thus obtained as $\Delta C \equiv C(T_O^-) - C(T_O^+) \simeq \frac{\alpha^2 T_O}{8\beta}[1 + \frac{4\gamma^2\chi_0}{\beta}(\chi_0 H)^2]$, taking $C(T_O^+) = 0$, where T_O^+ and T_O^- are the temperatures just above and below T_O.

[55] D. Aoki, Y. Homma, Y. Shiokawa, H. Sakai, E. Yamamoto, A. Nakamura, Y. Haga, R. Settai, and Y. Onuki, J. Phys. Soc. Jpn. **74**, 2323 (2005).

[56] F. Honda, N. Metoki, K. Kaneko, S. Jonen, E. Yamamoto, D. Aoki, Y. Homma, Y. Haga, Y. Shiokawa, and Y. Onuki, Phys. Rev. B **74**, 144413 (2006).

[57] Here, the Dzyaloshinsky-Moriya interaction may cause a helimagnetic order, but note that such an effect does not occur for the ZrNiAl structure [58], although URhSn has a noncentrosymmetric structure.

[58] M. Kataoka and O. Nakanishi, J. Phys. Soc. Jpn. **50**, 3888 (1981).

[59] Y. Kitano and T. Nagamiya, Prog. Theor. Phys. **31**, 1 (1964).

[60] B. R. Cooper, in *Phenomenological Theory of Magnetic Ordering: Importance of Interactions with the Crystal Lattice*, edited by R. J. Elliot, Magnetic Properties of Rare Earth Metals (Springer, New York, 1972).

[61] R. Shiina, O. Sakai, H. Shiba, and P. Thalmeier, J. Phys. Soc. Jpn. **67**, 941 (1998).

[62] T. Sakakibara, T. Tayama, K. Kitami, M. Yokoyama, K. Tenya, H. Amitsuka, D. Aoki, Y. Onuki, Z. Kletowski, T. Matsumura, and T. Suzuki, J. Phys. Soc. Jpn. Suppl. **69**, 25 (2000).

[63] T. Takeuchi, Y. Tokiwa, K. Sugiyama, R. Settai, Y. Haga, E. Yamamoto, T. Honma, K. Kindo, and Y. Onuki, Physica B **284-288**, 1285 (2000).

[64] Since only $\chi(T)$ and $C(T)$ data are not sufficient to clarify nine independent CEF parameters for the hexagonal ZrNiAl structure that should be taken as an orthorhombic symmetry (C_{2v}) [65, 66], inelastic neutron scattering experiments along with ultrasound measurements would be useful to clarify the CEF level scheme in URhSn.

[65] A. Szytuła, S. Baran, Ł. Gondek, A. Arulraj, B. Penc, and N. Stüsser, Acta Phys. Pol. **117**, 590 (2009).

[66] U. Walter, J. Phys. Chem. Solids **45**, 401 (1984).

[67] Y. Tanaka, T. Inami, T. Nakamura, H. Yamauchi, H. Onodera, K. Ohoyama, and Y. Yamaguchi, J. Phys.: Condens. Matter **11**, L505 (1999).

[68] K. Hirota, N. Oumi, T. Matsumura, H. Nakao, Y. Wakabayashi, Y. Murakami, and Y. Endoh, Phys. Rev. Lett. **84**, 2706 (2000).

[69] T. Onimaru, T. Sakakibara, N. Aso, H. Yoshizawa, H. S. Suzuki, and T. Takeuchi, Phys. Rev. Lett. **94**, 197201 (2005).

[70] K. Kuwahara, K. Iwasa, M. Kohgi, N. Aso, M. Sera, and F. Iga, J. Phys. Soc. Jpn. **76**, 093702 (2007).